Chemistry–A European Journal
Research Article
doi.org/10.1002/chem.202303013
Chemistry Europe
European Chemical Societies Publishing
www.chemeurj.org

VIP *Very Important Paper*

Cage Match: Comparing the Anion Binding Ability of Isostructural Versus Isofunctional Pairs of Metal-Organic Nanocages

Kaitlyn G. Dutton,[a] Taro J. Jones,[a] Thomas J. Emge,[a] and Mark C. Lipke*[a]

Affinities of six anions (mesylate, acetate, trifluoroacetate, *p*-toluenecarboxylate, *p*-toluenesulfonate, and perfluorooctanoate) for three related Pt^{2+}-linked porphyrin nanocages were measured to probe the influence of different noncovalent recognition motifs (e.g., hydrogen bonding, electrostatics, π bonding) on anion binding. Two new hosts of $M_6L_3^{12+}$ (**1b**) and $M_4L_2^{8+}$ (**2**) composition (M = (en)Pt^{2+}, L = (3-py)$_4$porphyrin) were prepared in a one-pot synthesis and allowed comparison of hosts that differ in structure while maintaining similar N–H hydrogen-bond donor ability. Comparisons of isostructural hosts that differ in hydrogen-bonding ability were made between **1b** and a related $M_6L_3^{12+}$ nanoprism (**1a**, M = (tmeda)Pt^{2+}) that lacks N–H groups. Considerable variation in association constants ($K_1 = 1.6\times10^3$ M^{-1} to 1.3×10^8 M^{-1}) and binding mode (*exo* vs. *endo*) were found for different host–guest combinations. Strongest binding was seen between *p*-toluenecarboxylate and **1b**, but surprisingly, association of this guest with **1a** was only slightly weaker despite the absence of NH···O interactions. The high affinity between *p*-toluenecarboxylate and **1a** could be turned off by protonation, and this behavior was used to toggle between the binding of this guest and the environmental pollutant perfluorooctanoate, which otherwise has a lower affinity for the host.

Introduction

Many types of nanoporous structures are capable of hosting one or more guest molecules,[1] such as aromatic compounds,[2] anions,[3] cations,[4] amino acids,[5] drug molecules,[6] and environmental toxins,[7] making porous hosts potentially useful for pollutant remediation,[8] chemical separations,[9] drug delivery,[10] catalysis,[11] and a variety of other applications.[12] In many cases, it is valuable to bind specific guests with high affinity ($\log K_a \geq 6$)[1c,13] and/or to control the uptake or release of guests,[14] motivating considerable interest in understanding features that influence the strength of guest binding. Anionic guests are interesting in this regard since cationic hosts[3a,c–g,k–m,o] provide an inherently high but non-specific electrostatic affinity for anions,[4a,b,e,15] while hydrogen bonding,[3a–h] anion-π interactions,[3g,h,n] π-stacking,[3f,m] solvophobic effects,[3e,l] and sterics[3i,k] can serve to modulate this affinity to increase or decrease the strength of binding for specific anions. A better understanding of the contributions from these various factors would benefit the design of receptors for specific anions, but there have been relatively few studies that have systematically examined how individual recognition motifs combine to influence overall anion binding strengths.[16]

Owing to their modularity,[1d,f,h,i,l,17] self-assembled metal-organic nanocages[1d–l] are optimal targets for preparing closely related hosts that allow the effects of individual structural or functional modifications to be assessed for their influence on anion binding. For example, different metal linkers or organic ligands can be used to alter chemical functionality,[1d,f,3d,k,18] and the metal-ligand stoichiometry can be altered to generate different structure types with varied pore sizes and geometries.[1i,19] Herein, we utilize these features to present a comparison of anion-binding in three porphyrin-walled nanocages that are held together by (*NN*)Pt^{2+} linkers (Scheme 1). We recently reported[20] the trigonal prismatic $M_6L_3^{12+}$ cage **1a** (M = (tmeda)Pt^{2+}, L = (3-py)$_4$porphyrin) based on a known Pd^{2+} linked structure-type,[2g,5d,19e] and found that **1a** binds PF_6^- anions in CD_3CN solution,[20a] motivating further examination of anion binding in this and related cages. Structural and functional comparisons were facilitated by preparing a closely related (en)Pt^{2+} linked $M_6L_3^{12+}$ cage (**1b**) and a smaller (en)Pt^{2+} linked $M_4L_2^{8+}$ cage (**2**), where strong Pt–N coordination enables isolation of these non-interconverting structures. The two M_6L_3 cages **1a,b** are isostructural, differing primarily by the presence (**1b**) or absence (**1a**) of NH groups in their (*NN*)Pt^{2+} linkers, while **2** is comprised of the same components as **1b** but has a cavity that is too small to bind guests internally. Thus, these cages provide two interesting comparisons: (1) isostructural hosts that share the same charge and pore geometry but differ in the availability of classic hydrogen-bond donors (**1a** vs. **1b**); and (2) isofunctional hosts that have similar hydrogen-bonding clefts but differ considerably in possible modes of guest binding (**1b** vs. **2**).

[a] *Dr. K. G. Dutton, T. J. Jones, Dr. T. J. Emge, Prof. Dr. M. C. Lipke*
Department of Chemistry and Chemical Biology
Rutgers University - New Brunswick
123 Bevier Road Piscataway NJ 08854 (USA)
E-mail: ml1353@chem.rutgers.edu

Supporting information for this article is available on the WWW under https://doi.org/10.1002/chem.202303013

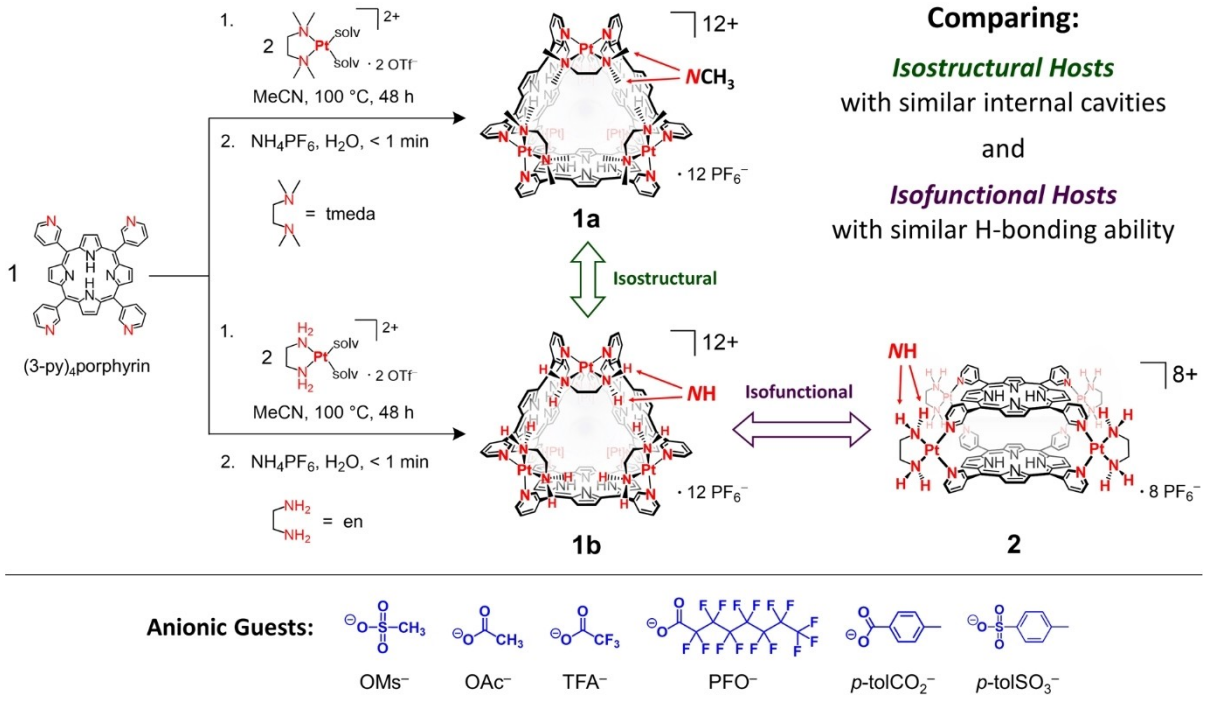

Scheme 1. (Top) Synthesis of isostructural and isofunctional Pt^{2+}-linked nanocage hosts; (bottom) the series of anions studied as guests for these hosts.

The three cages were examined as hosts for a library of six organic anions (Scheme 1) that were chosen to enable comparisons of different anion types (RCO_2^- vs. RSO_3^-), different basicities (e.g., acetate vs. trifluoroacetate), and substituents of different sizes and functionality (R=Me, CF_3, C_7F_{15}, *p*-tolyl). Most of the host-guest combinations display 1:2 noncooperative[21] binding based on ^{1}H NMR titrations,[22] with K_1 ranging from about 10^3 to 10^8 M^{-1}. As expected, strongest association was seen between the *p*-tolCO_2^- and *p*-tolSO_3^- guests and the hosts **1a,b** that can encapsulate the *p*-tolyl group, but surprisingly, the basicity of the anions and availability of NH hydrogen-bond donors has only a small (<1 order of magnitude) effect on the strength of binding.

In these studies, we employed a method[23] for measuring the strong association ($K_1 = 10^{7.4}$ M^{-1}) of *p*-tolCO_2^- in host **1a** whereby protonation of the guest with a weak acid is used to displace it from the host in an equilibrium that can be quantified by ^{1}H NMR spectroscopy. This proton-responsive host-guest behavior also allows affinity to be toggled reversibly between favoring the strongly binding *p*-tolCO_2^- anion and favoring the weakly binding perfluorooctanoate anion (PFO^-, $K_1 = 10^{3.2}$ M^{-1} in **1a**). Perfluorooctanoate is a common example of a polyfluorinated alkyl substance (PFAS), which are highly toxic environmental pollutants,[24] so the ability of **1a** to catch and release PFO^- may be valuable for future development of systems for environmental remediation.

Results and Discussion

Synthesis and Characterization of Nanoprisms 1b and 2

The new (en)Pt^{2+} linked nanocages **1b** and **2** were prepared from (3-py)$_4$porphyrin and [(en)Pt(NCMe)$_2$]OTf_2 (1.95 equiv.) in a one-pot synthesis using similar conditions (100 °C in MeCN for 48 h) to those[20a] used to prepare the (tmeda)Pt^{2+} linked cage **1a** (Scheme 1). Notably, **2**·8OTf is insoluble in MeCN, allowing facile isolation from other products before conversion to the more soluble PF_6^- salt via metathesis with NH_4PF_6 in MeOH. The trigonal cage **1b** was more challenging to isolate, requiring use of reverse phase chromatography and recrystallization from MeCN and ^{t}BuOMe to provide pure **1b**·12PF_6.

The new cages **1b** and **2** were identified by ^{1}H NMR spectroscopy (Figure 1), single-crystal XRD (see Figure 2 below), and ESI-HRMS (Figures S7-10). The ^{1}H NMR spectra of **1b** and **2** both show splitting of the porphyrin β-CH resonances into two signals, revealing the 2-fold symmetric environment of the porphyrin walls in each cage, just as observed for **1a**. Likewise, splitting of the ethylenediamine CH and NH resonances of **1b** and **2** is reminiscent of the *endo* vs. *exo* differentiation of the signals of the tmeda ligands in **1a.**[20a] The similar NMR splitting patterns and hydrodynamic radii of **1b** and **2** (see Figures S3,S6 for DOSY spectra) prevented unambiguous identification of each by NMR methods, so ESI(+)-HRMS was used to confirm the respective M_6L_3 and M_4L_2 compositions of **1b** and **2** (Figures S7-10).

It is worth noting that **2** is most likely a kinetically trapped product[25] since related (*NN*)Pd^{2+} linkers, which are more labile than their (*NN*)Pt^{2+} counterparts, react with (3-py)$_4$porphyrin to

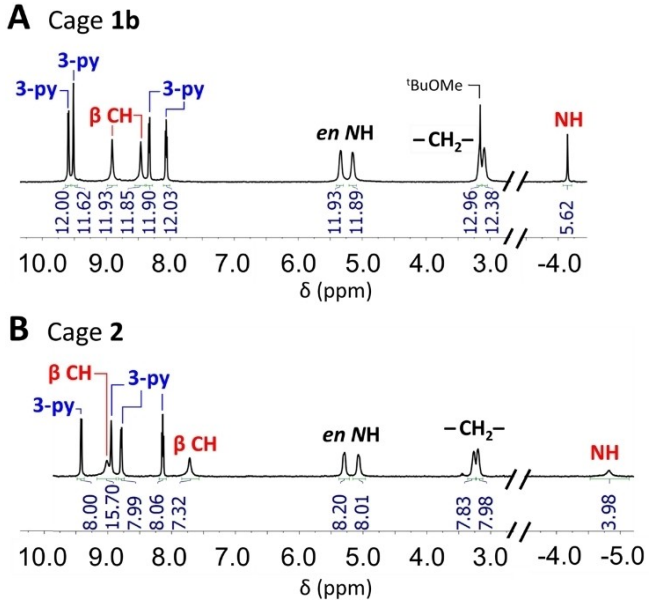

Figure 1. ^{1}H NMR spectra (500 MHz, CD_3CN, 298 K) of (A) **1b** and (B) **2**.

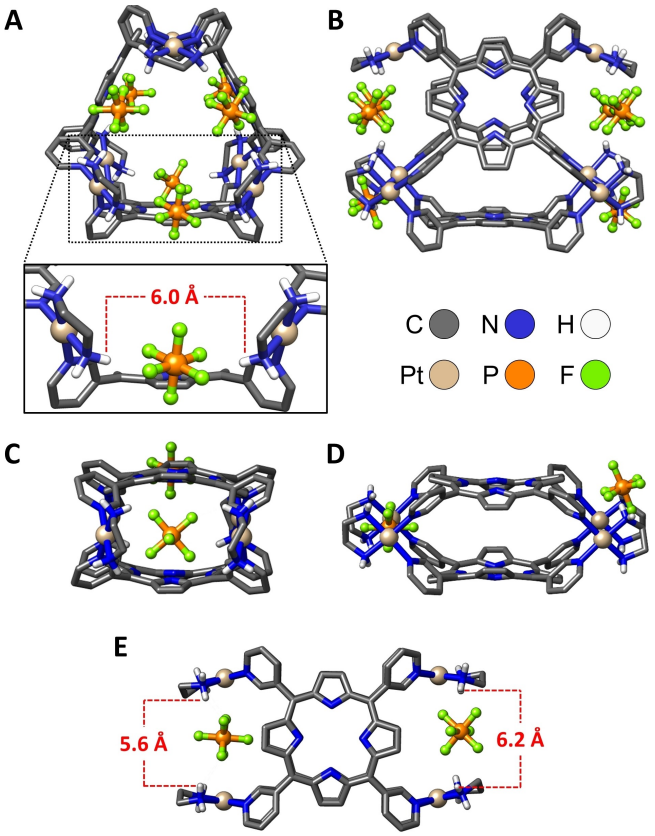

Figure 2. Solid-state structures of (A–B) **1b** and (C–E) **2** showing only the PF_6^- anions that associate closely with the apertures of the cages. Solvates, other anions, and hydrogen atoms are omitted for clarity, except for the NH positions of (en)Pt^{2+} groups. Representative NH–HN separations are labeled at the apertures of the cages. (A) View looking at a triangular face of **1b**, with an expansion showing one of the anion-binding pockets of the cage. (B) Side view of **1b** (orthogonal to A) showing anions associated at the edges of the cage. (C) View facing one of the anion-binding pockets of **2**. (D) Side view of **2** (orthogonal to C) showing different placements of disordered PF_6^- anions in the anion-binding pockets. (E) View facing one of the porphyrin walls of **2**, with NH···HN separations labeled at the claw-like anion-binding pockets of the cage.

give quantitative formation of triangular prisms[2g,5d,19e] analogous to **1a**,**b**, suggesting this M_6L_3 structure-type is thermodynamically favored. Nevertheless, **2** is stable enough that no conversion to **1b** was detected after >6 months under ambient conditions in CD_3CN. The discovery of **2** led us to examine whether other cages are produced in the synthesis of **1a**, which forms in ~50% in situ yield alongside multiple byproducts.[20a] However, we were unable to isolate or identify by ESI(+)-HRMS any other cages formed in the synthesis of **1a**, though these efforts did have the benefit of improving chromatographic methods for isolating **1a**, increasing the yield of pure **1a** to 24%, more than doubling our previously reported yield of 10% (see Supporting Information).

The structures of **1b** and **2** (Figure 2) were determined by X-ray diffraction analysis on single crystals grown by vapor diffusion of ^{t}BuOMe or $^{i}Pr_2O$ into MeCN solutions of **1b**·12PF_6 or **2**·8PF_6. The structure of **1b** (Figure 2A,B) confirms it is a triangular prism analogous to **1a**, maintaining a cavity with a comparable width (porphyrin centroid-to-centroid distances of 8.1–9.1 Å for **1a**; 8.7–9.3 Å for **1b**) and length (18.5 Å, **1a**; 18.6 Å, **1b**). However, the (en)Pt^{2+} linkers of **1b** eliminate steric crowding at the apertures of **1a** caused by the *N*CH_3 groups. This allows three PF_6^- anions to sit at similar depths in each aperture of **1b** (Figure 2B), whereas our reported structure of **1a**·12PF_6 has one PF_6^- anion situated fully inside each end of the cage while the other anions are pushed fully outside.[20a] An NH···HN cleft of ~6 Å surrounds each PF_6^- anion at the apertures of **1b**, providing two short NH···F contacts (2.0–2.2 Å, Figures 2A and S14) for each anion, consistent with strong hydrogen bonding. Thus, **1b** appears to significantly alter the anion-recognition motif of **1a** despite the otherwise similar structures of these two cages.

The solid-state structure of **2** (Figure 2C–E) shows that the (en)Pt^{2+} linkers are oriented to provide an approximately 2-fold symmetric environment for the porphyrin walls,[26] consistent with NMR characterization. Notably, the porphyrin macrocycles exhibit pronounced saddling,[27] which is needed to accommodate nearly ideal 90° py-Pt-py angles at the linkers. These distortions likely contribute to the lower thermodynamic stability of this M_4L_2 structure relative to the M_6L_3 cages **1a**,**b**, which have nearly planar porphyrin walls. The extended packing of **2** (Figure S16) reveals continuous stacks of the cages with the porphyrin walls of neighboring cages separated by a distance (~3.6 Å) consistent with expected Van der Waals contacts, while the placement of the (en)Pt^{2+} groups is staggered for adjacent cages.

Of the most salience for anion binding, the internal cavity of **2** is too small to accommodate any guests larger than an acetonitrile solvate, while the [(en)Pt]$^{2+}$ linkers are arranged to create two claw-like pockets each lined with four NH bonds separated by NH–HN distances of 5.6–6.2 Å (Figure 2E). Thus, **2** is unlikely to fully encapsulate most guests, but it retains external recognition sites that should be at least as effective at

hydrogen-bonding as the anion-binding pockets of **1b**. Indeed, the sites between the $[(en)Pt]^{2+}$ linkers of **2** are partially occupied with PF_6^- anions that can engage in up to four NH···F contacts with H···F distances ranging from 2.0 to 3.0 Å.

Nanocages as Hosts for Anionic Guests

The affinity of hosts **1a**, **1b**, and **2** for anions was investigated in CD_3CN using the carboxylate and sulfonate guests shown in Scheme 1. All of these anions should have similar electrostatic affinity for the cationic hosts, while different host-guest combinations vary in possible hydrogen bonding, π stacking, solvophobic, and steric interactions, allowing the influence of these features to be scrutinized. The strength, stoichiometry, and *exo* vs. *endo* geometry of anion binding is summarized in Scheme 2 and Table 1 for each host-guest combination, as determined by a variety of titration and competition experiments monitored by ^{1}H NMR spectroscopy in CD_3CN (see below). It is worth noting that the hosts likely maintain an affinity for their PF_6^- counterions in solution,[20a] so the association constants in Table 1 represent affinities of guests in competition with PF_6^-. Our titrations were designed to allow the PF_6^- concentration to be treated as a constant during analysis of the results (i.e., displacement of PF_6^- from the hosts is matched approximately to dilution of the samples to maintain $[PF_6^-] \approx 10$ mM), but as a result, the K_1 and K_2 values in Table 1 are only strictly valid for ~1 mM solutions of the hosts.

The *endo* placement and maximum 1:2 stoichiometry of anion binding was clearest for association of *p*-$tolCO_2^-$ and *p*-$tolSO_3^-$ in **1a** since these guests exhibit slow exchange between bound and unbound states on the NMR timescale (Figures 3, S40–42, and S45–47). Signals of the 1:1 complexes were apparent after adding just 0.1 equiv. of either *p*-tolyl guest to **1a**, with all the resonances of the guests shifted upfield (e.g., CH_3 signals at ≤ -5 ppm) as expected for binding inside a porphyrin-walled cavity. New sets of cage signals also appeared for the 1:1 complex, with the greatest changes relative to empty **1a** observed for the inward facing CH positions of the tmeda and pyridyl moieties, the latter of which is split into two distinct singlets by occupancy of just one of the two anion-binding sites. As the titrations progressed, signals of the 1:1 complexes grew in and then gave way to the signals of the symmetric 1:2 complexes, with a statistical mixture of 1:1 and 1:2 complexes observed after 1 equiv. of *p*-$tolCO_2^-$ or *p*-$tolSO_3^-$ had been added, indicating noncooperative binding (note that $K_2 = K_1/4$ for noncooperative binding).[21] The 1:1 and 1:2 host-guest complexes were also observable in the gas phase by ESI(+)-HRMS (Figures S127-128). However, association of *p*-$tolCO_2^-$ and *p*-$tolSO_3^-$ with **1a** was too strong ($K_1 > 10^5$ M^{-1}) to directly measure by NMR methods, necessitating use of competition experiments (see below).

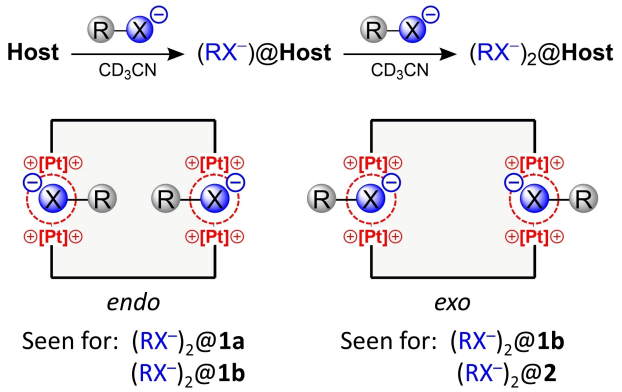

Scheme 2. (Top) Sequential association of two anionic guests with hosts **1a,b** or **2**. (Bottom) Schematic depiction of possible placement (*endo* vs. *exo*) of the R-groups of anions interacting with **1a,b** and **2**.

Table 1. Summary of association constants and geometry (*endo* vs. *exo*) for anionic guests interacting with hosts **1a,b** and **2**.

Anion	$\log K_1$, $\log K_2$,[a] and geometry of anion binding in:		
	1a	**1b**	**2**
OMs^-	3.70; 3.10 *endo*	*exo*[b]	3.83; 3.23 *exo*
OAc^-	4.30; 3.70 *endo*	*exo*[b]	N/A[c]
TFA^-	3.72; 3.11 *endo*	*exo*[b]	3.95; 3.35 *exo*
PFO^-	3.21[d] *endo*	*exo*[b]	3.81; 3.20 *exo*
p-$tolCO_2^-$	7.37; 6.78 *endo*	8.12; 7.52 *endo*	N/A[c]
p-$tolSO_3^-$	7.48; 6.88 *endo*	7.92; 7.32 *endo*	3.90; 3.30 *exo*

[a] K_1 and K_2 refer to sequential association of anions in a 1:2 noncooperative binding model unless noted otherwise; [b] Association could not be reliably quantified due to poorly defined stoichiometry of binding; [c] Association could not be quantified due to partial deprotonation of the ethylenediamine NH bonds by the anionic guest; [d] This host-guest combination provides only a 1:1 complex.

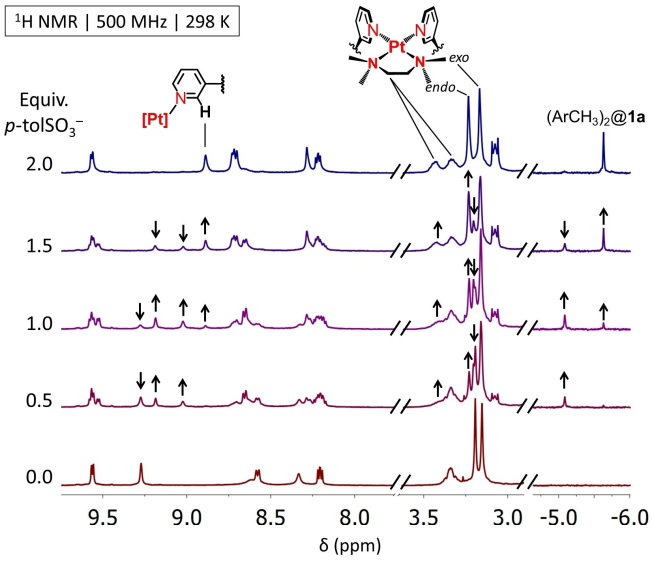

Figure 3. Truncated ^{1}H NMR spectra (500 MHz, CD_3CN, 298 K) acquired during a titration of *p*-$tolSO_3^-$ into a solution of **1a**. Resonances of the host that change the most are labeled and correspond to CH positions near the apertures of the cage (the tmeda ligand) or fully inside the cage (the pyridyl 2-position). The CH_3 resonance of the bound *p*-$tolSO_3^-$ guests in the 1:2 complex is also labeled. For clarity, the vertical scaling of the most upfield region (−5 to −6 ppm) was increased relative to the other regions of the spectra.

Both *p*-tolyl anions exchange rapidly in and out of **1b** on the NMR timescale (Figures S83 and S89), requiring a careful analysis of the spectra produced by these host-guest combinations. Titration of *p*-tolSO$_3^-$ into **1b** initially results in shifts of the pyridyl 2-position CH resonance and one of the ethylenediamine NH resonances of **1b** (Figure S89), corresponding well to the signals that change the most for binding of this anion in **1a**. However, the pyridyl 2-position signal of **1b** reaches its final value ($\Delta\delta = -0.42$ ppm) after slightly more than 2 equiv. of *p*-tolSO$_3^-$ have been added, while the NH signal moves steadily ($\Delta\delta = +2.22$ ppm) over the course of adding >7 equiv. of the anion, implying more than one binding mode causes these changes. The movement of the pyridyl signal is attributed to *endo* association of up to two *p*-tolSO$_3^-$ anions in **1b**, while shifts of the NH signal are attributed to both the 1:2 *endo* binding mode and a weaker *exo* binding of additional anions, as might be expected based on association of six PF$_6^-$ anions with the apertures of this host in the solid state. The structural similarity of **1b** to **1a** suggests that *endo* binding of two *p*-tolSO$_3^-$ in **1b** should be non-cooperative as was found for **1a**, but it was not as straightforward to confirm this for **1b** since individual 1:1 and 1:2 complexes could not be observed for interaction of **1b** and *p*-tolSO$_3^-$. Instead, shifts of the pyridyl 2-position resonance of **1b** were used to construct a Job plot (Figure S93), which supports the assignment of non-cooperative binding of two *p*-tolSO$_3^-$ in **1b**. Comparison of these results with those from titrating **1b** with *p*-tolCO$_2^-$ (Figure S83) suggests that both *p*-tolyl guests show similar interactions with this host. As with **1a**, competition experiments were needed to quantify the strength of these anions binding inside **1b** (see below).

The smaller anions OMs$^-$, OAc$^-$, and TFA$^-$ exchange rapidly in and out of **1a** on the NMR timescale (Figures 4A and S17-34), and all six anions exhibit fast exchange kinetics with hosts **1b** and **2** (Figures 4B and S58–122). Bindfit was used to determine association constants from the NMR titration data for these host–guest combinations,[28] though reliable analyses were possible for only about half these examples. Deprotonation of the NH groups of **2** by OAc$^-$ and *p*-tolCO$_2^-$ prevented assessment of host–guest interactions in these two cases (Figures S101–102 and S114–115), and as already noted, the binding of *p*-tolCO$_2^-$ and *p*-tolSO$_3^-$ in **1b** was too strong ($K_1 > 10^5$ M^{-1}) to analyze directly.[22] For the remaining examples, a 1:2 noncooperative binding model provided the best fitting of the titration data, qualitatively matching the behavior of the *p*-tolyl guests with **1a**. However, all of the anions cause changes to the ethylenediamine NH signal of **1b** that match those resulting from titration with >7 equiv. *p*-tolSO$_3^-$, suggesting more than two equivalents of each anion interact with **1b**. This complex and uncertain stoichiometry prevented reliable quantification of the strengths of smaller anions interacting with **1b** (see Figures S60, S67, S73, and S79).[22]

Of the small anions, the low basicity and good ^{1}H NMR handle of OMs$^-$ make this guest the best suited for comparing the three hosts. Titration of OMs$^-$ into a solution of **1a** resulted initially in only slight movement of most of the ^{1}H NMR signals of the cage, except for the resonances corresponding to the 2-position of the pyridyl groups and to one of the *N*CH$_3$ resonances of the tmeda ligands, which respectively shift by +0.3 ppm and +0.1 ppm (Figure 4A). These signals represent the only CH positions facing the interior of **1a**, suggesting *endo* association of the OMs$^-$ guests. Likewise, the CH$_3$ resonance of OMs$^-$ is initially observed at 0.23 ppm, which is 2.18 ppm upfield of its shift (δ 2.41 ppm) in a reference solution of [TBA][OMs], suggesting the anion binds inside **1a**. This CH$_3$ signal moves steadily downfield as excess OMs$^-$ is added, consistent with fast exchange between the free and bound guest. The 6-position CH signal of the pyridyl groups, which faces the exterior of **1a**, also begins shifting as an excess of OMs$^-$ accumulates, which can be attributed to *exo* association of the anion with **1a** once internal anion-binding sites become saturated. This behavior was observed for the interaction of all anions with **1a** as internal binding sites approach saturation, but since *exo* association does not appear close to saturated

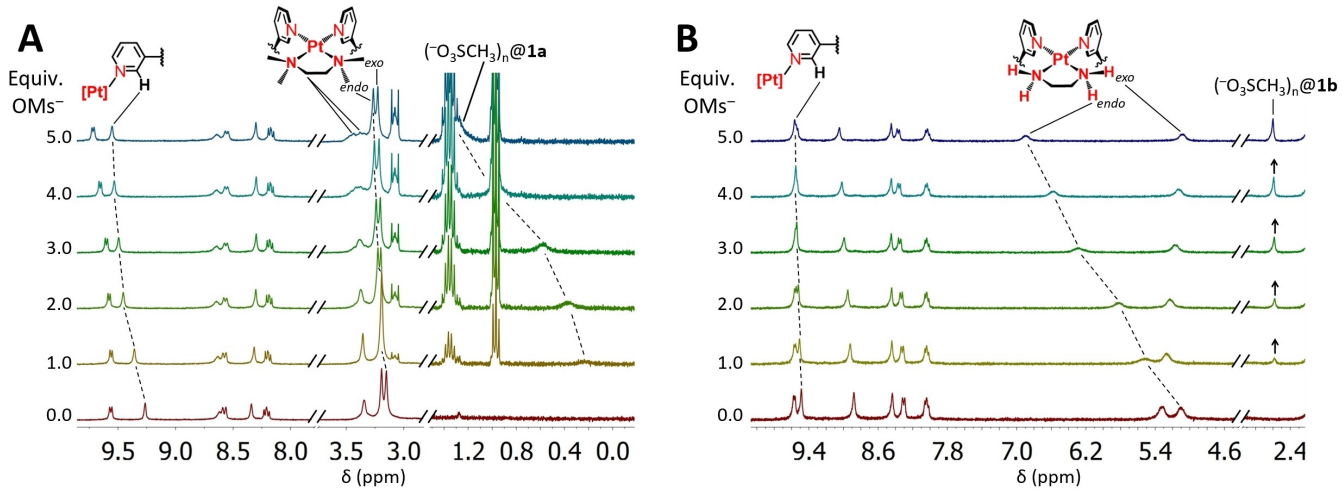

Figure 4. Truncated ^{1}H NMR spectra (300 MHz, CD$_3$CN, 298 K) acquired during titrations of OMs$^-$ into hosts (A) **1a** and (B) **1b**. Select resonances of the hosts are labeled and correspond to signals that change the most during the titrations. Resonances of the guest are also labeled in each set of spectra. Note that the vertical scaling is increased in the upfield region (0.0 to 1.2 ppm) of (A) to improve visibility of the broad guest resonance.

even after adding an excess of the anions (>10 equiv., Figure S19), we did not further investigate these weak interactions.

Titrations of **1b** and **2** with OMs^- reveal that one of the ethylenediamine NH signals of each host shifts considerably downfield ($\Delta\delta \approx +2$ ppm; Figures 4B, S59, and S97), suggesting that the anion interacts with the inward facing NH bonds of these hosts. Thus, NH···O hydrogen-bonding occurs as expected, but these interactions do not appear to provide higher affinity of OMs^- for **1b** or **2** vs. **1a**. The strengths of OMs^- binding in **1a** and **2** were quantified using Bindfit to reveal $K_1 = 5.01\times10^3\ M^{-1}$ for **1a** (Figure S20) and $K_1 = 6.72\times10^3\ M^{-1}$ for **2** (Figure S98), revealing comparable binding strengths with these hosts. A reliable analysis of the binding of OMs^- to **1b** was not possible, but it was noted that the CH_3 resonance of OMs^- remains near its unbound value of 2.41 ppm during titrations into **1b** or **2**, suggesting *exo* orientation of the CH_3 group upon association with either host. Given the similar mode of association and similar hydrogen-bonding pockets of **1b** and **2**, it is likely that OMs^- binds with similar strength to **1b** as it does with **2**, and by extension, with **1a**. The ability of **1a** to encapsulate the CH_3 substituent of OMs^- might compensate for the absence of NH–O hydrogen bonding. Likewise, CH···O hydrogen bonding with the inward-facing pyridyl 2-position CH bonds of **1a** may also offset the lack of traditional hydrogen-bond donors in this host.

The other small anions OAc^- and TFA^- show similar host–guest interactions with **1a** as were characterized for OMs^-, including a limiting 1:2 stoichiometry for *endo* association. Association of OAc^- inside **1a** was indicated by the upfield shift of the CH_3 signal (Figure S24), and ^{19}F NMR spectroscopy was used to confirm *endo* association of TFA^- (Figure S33). A 4-fold higher affinity was determined for binding OAc^- ($K_1 = 2.00\times10^4\ M^{-1}$, Figure S26) than OMs^-, while TFA^- binds with comparable affinity ($K_1 = 5.21\times10^3\ M^{-1}$, Figures S31) to that of OMs^-, suggesting that basicity of the anions contributes to the strength of their interactions with **1a**. However, the enhancement of binding for OAc^- is modest despite the ≥11 pK_a unit difference between its conjugate acid and those of OMs^- or TFA^-.[31]

The basicity of OAc^- complicated the characterization of its interactions with **1b** and **2**. The inward-facing NH resonance of each host broadens and then disappears during titrations of these cages with acetate (Figures S65 and S101), suggesting that deprotonation of the $[(en)Pt]^{2+}$ linkers is competitive with anion binding. However, changes to other resonances of **1b** were consistent with anion association (Figure S66) that is similar in strength and character to that observed for the interactions of OMs^- to this host. Titrations of **1b** and **2** with TFA^- or PFO^- (Figures S71–82, S103–113) also result in host-guest behavior similar to that characterized between these hosts and OMs^-, including similar association constants (Table 1). The ^{19}F NMR spectra from these titrations showed only small changes to the fluorine resonances of the bound guests ($\Delta\delta_{19F} < 0.5$ ppm, Figures S75, 81, 107), which suggests that both fluorinated anions exhibit *exo* association with **1b** and **2**, explaining why the CF_3 vs. C_7F_{15} groups do not substantially influence the strengths of association. Likewise, *p*-$tolSO_3^-$ binds outside host **2** (Figures S116–120), resulting in similar affinity to that quantified for the binding of other anions to **2** (Table 1).

While PFO^- and TFA^- have similar host–guest interactions with **1b** and **2**, the PFO^- anion differs considerably from TFA^- in its interactions with **1a**. This combination was the sole example that showed a maximum 1:1 stoichiometry, as evident from the appearance of just a single set of new host-guest ^1H NMR signals during titration of **1a** with PFO^- even after adding >12 equiv. of the anion (Figure S35-36). Several resonances of **1a** are split into two signals for its complex with PFO^- (Figure S35-36), consistent with desymmetrization of the cage by association of a carboxylate group in just one of the two anion-binding pockets. These results suggest *endo* binding of PFO^- in **1a** since the inability of the cavity to fit more than one C_7F_{15} chain would explain the binding of a single guest. The *endo* association of PFO^- was further supported by the observation of distinct ^{19}F NMR signals for the terminal CF_3 groups of the bound (−84.8 ppm) and unbound (−80.9 ppm) PFO^- anions (Figure S38), suggesting the chemical environment of the CF_3 is altered significantly in the complex. Since PFO^- exchanges slowly between bound/unbound states, its association constant with **1a** was determined by integration of several spectra during the titration, revealing $K = 1.62\pm0.10\times10^3\ M^{-1}$. The lower affinity of PFO^- vs. TFA^- for **1a** suggests the C_7F_{15} group of PFO^- does not interact very favorably with the cavity of this host.

Competition and Guest-Switching Studies

The affinity of hosts **1a**,**b** for *p*-$tolSO_3^-$ and *p*-$tolCO_2^-$ was too high ($K_1 > 10^5\ M^{-1}$) to quantify by NMR methods.[29] However, since the cages do not bind *p*-$tolCO_2H$ and the pK_a of this acid is known ($pK_a = 21.9$ in MeCN),[30] we were able to extract the host-guest association constant from the equilibrium for displacing *p*-$tolCO_2^-$ from the cages by protonation with a weak acid. Cage **1a** was selected for these experiments since the slow exchange kinetics of *p*-$tolCO_2^-$ with this host permits direct quantification of liberated *p*-$tolCO_2H$ by integration of its ^1H NMR resonances. As expected, titration of $[Et_3NH][BF_4]$ ($pK_a = 18.82$ in MeCN)[31] into a solution of (*p*-$tolCO_2^-)_2$@**1a** in CD_3CN resulted in release of *p*-$tolCO_2H$ (Figures 5 and S44), and the resulting host–guest and acid-base equilibria were deconvoluted to reveal very strong binding of *p*-$tolCO_2^-$ in **1a** ($K_1 = 2.37\pm0.09\times10^7\ M^{-1}$; see Scheme S1 and Table S3 in the Supporting Information for details of this analysis).

After quantifying the affinity between *p*-$tolCO_2^-$ and **1a**, a series of competition experiments were used to measure the remaining association constants for binding of *p*-$tolCO_2^-$ and *p*-$tolSO_3^-$ in **1a**,**b**. First, a "Guest Match" experiment was conducted to examine competition between *p*-$tolCO_2^-$ and *p*-$tolSO_3^-$ for binding in **1a**. Titration of the sulfonate guest into a solution of (*p*-$tolCO_2^-)_2$@**1a** led to the appearance of the ^1H NMR signals of (*p*-$tolSO_3^-)_2$@**1a** as well as a mixed-guest complex (*p*-$tolCO_2^-$)(*p*-$tolSO_3^-$)@**1a** (Figures 6 and S49-52), the latter of which was evident from upfield-shifted aryl CH resonances (δ −0.66, −1.00 ppm) that are distinct from those of

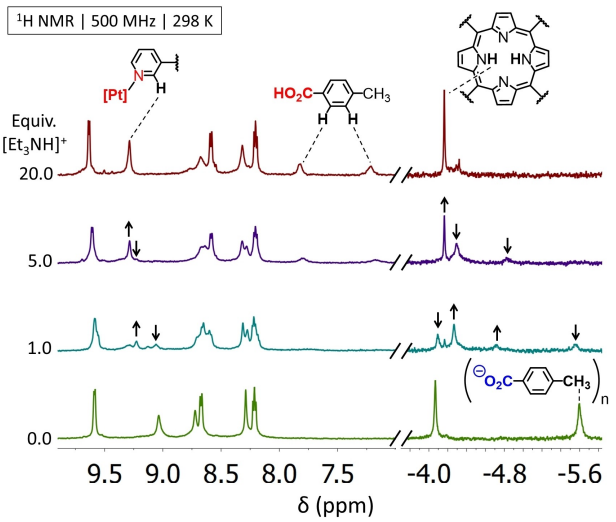

Figure 5. Truncated ^{1}H NMR spectra (500 MHz, CD_3CN, 298 K) acquired during the titration of $[Et_3NH][BF_4]$ into a solution of $(p\text{-tolCO}_2^-)_2$@**1a**. Select resonances are labeled to show the disappearance of signals of the host-guest complex and the appearance of signals of free **1a** and p-$tolCO_2H$.

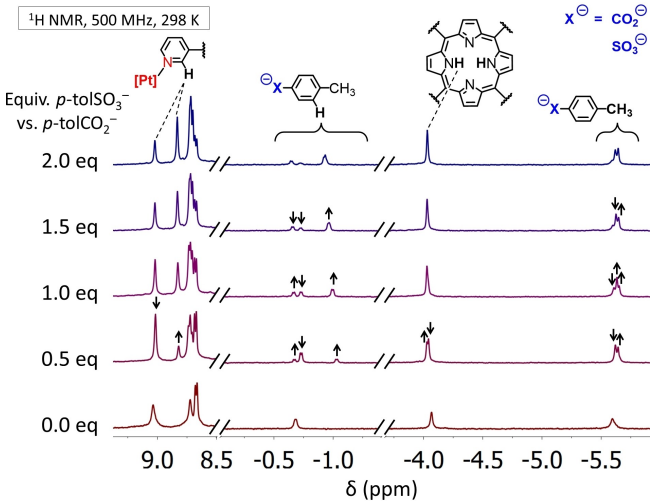

Figure 6. Truncated ^{1}H NMR spectra (500 MHz, CD_3CN, 298 K) acquired during the titration of p-$tolSO_3^-$ into a solution of $(p\text{-tolCO}_2^-)_2$@**1a**. Black arrows indicate growth and/or decay of signals of the initial host guest complex, the mixed-guest complex $(p\text{-tolCO}_2^-)(p\text{-tolSO}_3^-)$@**1a**, and $(p\text{-tolSO}_3^-)_2$@**1a**.

the encapsulated p-$tolCO_2^-$ (δ −0.73 ppm) and p-$tolSO_3^-$ (δ −1.32 ppm) guests in their individual 1:2 complexes with **1a**. The signals of the bound guests were integrated for several spectra acquired during the titration, revealing a slight preference for binding of p-$tolSO_3^-$ in **1a** ($K_1 = 3.05 \pm 0.05 \times 10^7$ M^{-1}).

The association constants for p-$tolCO_2^-$ and p-$tolSO_3^-$ binding in **1b** were determined by "Cage Match" competition experiments that measured the relative affinities of each anion for hosts **1a** vs. **1b**. In these experiments, equimolar solutions of **1a** and **1b** were titrated with p-$tolCO_2^-$ or p-$tolSO_3^-$ and the occupancies of the hosts were evaluated by ^{1}H NMR spectroscopy after each addition (see Figures S87–88, S94–95). Both p-tolyl anions showed higher affinity for **1b** than for **1a**, with p-$tolSO_3^-$ having a slight preference (2.75×) for **1b** over **1a**, which is increased just modestly (to 5.6×) for p-$tolCO_2^-$ binding in these cages (Table 1). Though the association between p-$tolCO_2^-$ and **1b** ($K_1 = 1.33 \times 10^8$ M^{-1}) is the strongest measured in this study, it is more notable that p-$tolCO_2^-$ and p-$tolSO_3^-$ show only weak preferences for **1b** vs. **1a** despite NH hydrogen-bond donors defining the anion-binding sites of **1b**. Thus, NH···O hydrogen bonding provides surprisingly weak enhancement of the overall interaction between anions and **1b**, suggesting that other factors are more important for anion recognition by **1a**,**b**, or that the multiple CH···O hydrogen bonds available in **1a** compensate effectively for the lack of traditional hydrogen-bond donors.

Another interesting result from comparing the affinities of p-$tolCO_2^-$ and p-$tolSO_3^-$ for **1a**,**b** is that the basicity of the anions has almost no effect on their strengths of association. We reasoned that this feature, along with the H^+ responsive binding of p-$tolCO_2^-$, could be harnessed to toggle between association of this strongly bound guest and the weakly binding but even more weakly basic PFO^- anion (Scheme 3). Indeed, addition of two equivalents of the acid PFOA to a solution of $(p\text{-tolCO}_2^-)_2$@**1a** resulted in ejection of both p-$tolCO_2^-$ guests, as evident from the disappearance of the ^{1}H NMR signals of the initial host-guest complex and appearance of resonances for free p-$tolCO_2H$ (Figure S53–54). Signals corresponding to (PFO^-)@**1a** were also observed, confirming capture of PFO^- by **1a**.

Since displacement of the two p-$tolCO_2^-$ required two equivalents of PFOA but only one PFO^- can bind in **1a**, we also performed an experiment in which a mixture of $(p\text{-tolCO}_2^-)_2$@**1a** and 1 equiv. PFO^- was treated with a small excess of lutidinium (2.1 equiv.) as an H^+ source, resulting in the release of p-$tolCO_2H$ and uptake of PFO^- into **1a**. Subsequent addition of an excess of Et_3N (45 equiv.) restored the initial $(p\text{-tolCO}_2^-)_2$@**1a** complex, necessarily resulting in release of PFO^- (Figures S55–57). Thus, the acid-responsive binding of p-$tolCO_2^-$ can be used to mediate the uptake and then release of PFO^-, which may be useful for removal of this pollutant from the environment and/or industrial waste streams.

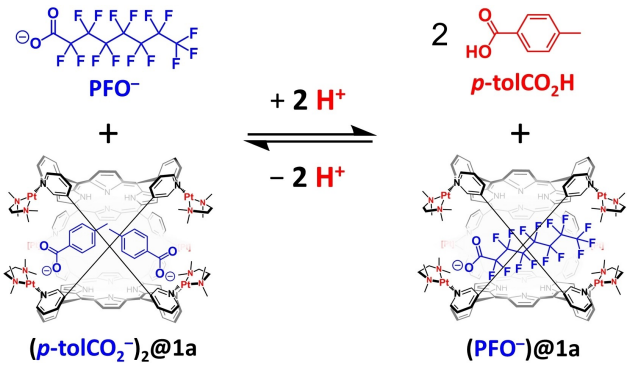

Scheme 3. Reversible uptake and release of PFO^- by **1a** using an acid stimulus.

DFT Analysis of Host-guest Interactions

Complexes of the anionic guests bound in **1a**,**b** and **2** could not be obtained as single crystals of sufficient quality for XRD analysis, so DFT calculations were performed to provide insight into how geometric factors influence anion binding. Optimizations of **1a** and **1b** in the absence of anions provided similar internal cavities with approximately D_{3h} symmetry (Figure S140). The tmeda ligands partially obscure the apertures of **1a**, consistent with the solid-state structure of this cage as its PF_6^- salt.[20a] However, **1a** takes on C_{2v} symmetry in the experimental structure, likely due to two anions that bind deeply in the apertures, lowering the symmetry. Indeed, optimization of **1a** and **1b** with two bound *p*-tolSO$_3^-$ anions provided approximately C_{2v} structures in both cases (Figure 7). The placement of the SO_3^- groups in the apertures of each cage is similar to the placement of PF_6^- anions in the experimental structures, featuring CH···O hydrogen bonding for **1a** and NH···O hydrogen-bonding for **1b**.

The different anion-recognition motifs of (*p*-tolSO$_3^-$)$_2$@**1a** and (*p*-tolSO$_3^-$)$_2$@**1b** result in slightly different placements of the *p*-tolyl groups inside the two cages (Figure 7). In (*p*-tolSO$_3^-$)$_2$@**1a**, the sulfonate group of each guest is bound deep in the apertures (Figure 7A) where it engages in four CH–O hydrogen bonds (D_{CH-O} = 1.9–2.4 Å) with the 2-position CH bonds of the pyridyl groups of the host (Figure 7B). This placement of the sulfonate groups requires that the *p*-tolyl groups of the guests take on an acute angle (76.4°, Figure 7A) relative to each other in order to both fit inside the host. In contrast, (*p*-tolSO$_3^-$)$_2$@**1b** has each sulfonate group engaged in three NH–O hydrogen bonding interactions ($D_{NH\cdots O}$ = 1.8–1.9 Å), which result in shallower placement of the anionic groups and a wider angle between the *p*-tolyl groups (113.3°, Figure 7C). An interesting result of the different *p*-tolSO$_3^-$ placements is that there is greater overlap between the aromatic surfaces of the host and guests in (*p*-tolSO$_3^-$)$_2$@**1a** than in (*p*-tolSO$_3^-$)$_2$@**1b**, which in turn, appears to cause host **1a** to take on a narrower conformation than **1b** in these complexes, as measured by the centroid-to-centroid spacings between the two closest porphyrins of each host (6.70 Å vs. 7.02 Å, Figures 7B,D). These results suggest that stronger π-π interactions in (*p*-tolSO$_3^-$)$_2$@**1a** might effectively offset the stronger NH···O hydrogen bonding available in (*p*-tolSO$_3^-$)$_2$@**1b**, thus explaining the similar affinities of each of these hosts for aromatic guests. It is worth noting that these computational results are corroborated by ^{1}H NMR data showing a more upfield shift of the signal of the ArCH$_3$ groups in (*p*-tolSO$_3^-$)$_2$@**1a** (δ_{CH3} = −5.71 ppm, Figure 4) than in (*p*-tolSO$_3^-$)$_2$@**1b** (δ_{CH3} = −3.30 ppm, Figure S90), consistent with the placement of these methyl groups closer to the center of the porphyrin walls in the complex with **1a**.

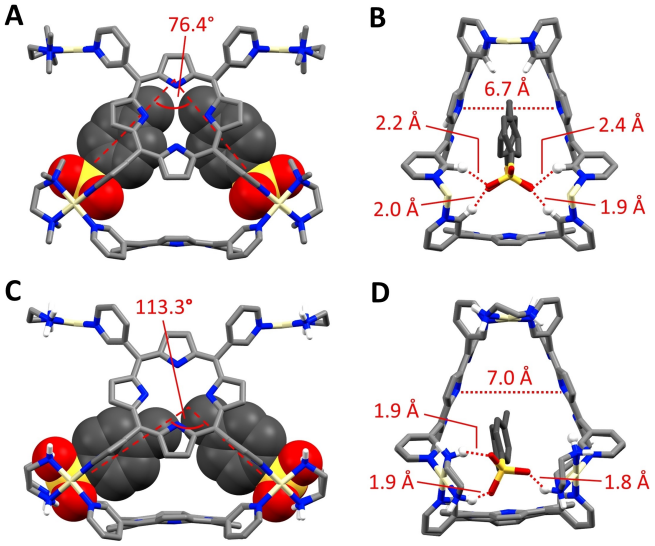

Figure 7. Computationally optimized structures of (A,B) (*p*-tolSO$_3^-$)$_2$@**1a** and (C,D) (*p*-tolSO$_3^-$)$_2$@**1b**. Hydrogen atoms are omitted for clarity except for those involved in interactions with the guests. (A) Side view of (*p*-tolSO$_3^-$)$_2$@**1a** illustrating the angle between the long axes of the two guests. (B) View of a triangular face of (*p*-tolSO$_3^-$)$_2$@**1a** with the tmeda ligands omitted to enable a clear view of the CH–O contacts between the pyridyl groups of the host and the SO_3^- group of a guest. (C) Side-view of (*p*-tolSO$_3^-$)$_2$@**1b** illustrating the angle between the long axes of the two guests. (D) View of a triangular face of (*p*-tolSO$_3^-$)$_2$@**1b** with NH···O contacts indicated between the host and a guest.

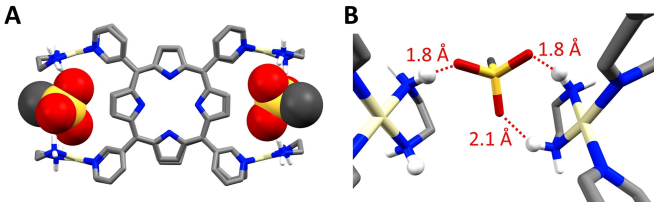

Figure 8. Computationally optimized structure of (OMs$^-$)$_2$@**2**. Hydrogen atoms are omitted for clarity, except for those of the (en)Pt^{2+} linkers. (A) View of (OMs$^-$)$_2$@**2** illustrating the *exo* placement of the CH_3 groups of the OMs$^-$ guest. (B) View from inside the host cavity of (OMs$^-$)$_2$@**2** depicting the NH···O contacts between the host and a guest.

The structure of (OMs$^-$)$_2$@**2** was also optimized (Figure 8) for comparison of its anion-binding motif with those of **1a**,**b**. Each sulfonate interacts closely (1.7–2.2 Å) with three NH donors on the host (Figure 8B), similar to the hydrogen-bonding seen in the optimized structure of (*p*-tolSO$_3^-$)$_2$@**1b**. The methyl groups of the guests in (OMs$^-$)$_2$@**2** point away from the porphyrin cavity of the host, consistent with experimental findings that the R groups of the anions do not have much effect on the strengths of their interactions with **2**. Indeed, DFT optimization of (*p*-tolSO$_3^-$)$_2$@**2** (Figure S139) yielded an anion-binding motif very similar to that found for (OMs$^-$)$_2$@**2**.

Conclusions

Two new nanocage hosts (**1b** and **2**) were obtained via one-pot synthesis, and their affinities for a series of anionic guests were compared to those of a previously reported nanocage **1a**. Hosts **1a** and **1b** are isostructural, both bearing large cavities capable of accommodating guests but differing in their hydrogen-bond-donor ability at the (*NN*)Pt^{2+} linkers. Host **2** is composed of a smaller number of the same components as **1b**, resulting in a host with similar hydrogen-bond donor groups but a cavity too small to accommodate guests internally. Key findings are: (1)

trends in *endo* vs. *exo* association of guests match expectations based on the solid-state structure of each host; (2) NH vs. CH hydrogen-bonding has a surprisingly weak influence on the strengths of anion binding by **1a** vs. **1b**; and (3) the basicities of the guest anions also has a weak influence on their binding, while π-π interactions and/or solvophobic effects have large influences. These latter observations led to the realization that the high affinity between *p*-tolCO_2^- and **1a** could be disabled by addition of an acid stimulus, which toggles off affinity for the strongly binding anions and activates affinity for less basic guests. This catch-and-release system was tested successfully for binding and release of PFO^-, suggesting a possible approach for developing reusable systems for the capture of this environmental toxin.

Supporting Information

The authors have cited additional references within the Supporting Information.[32–45]

Acknowledgements

The authors acknowledge the National Science Foundation (CHE award # 2204045) for financial support of this research; the Office of Advanced Research Computing (OARC) at Rutgers, The State University of New Jersey, for providing access to the Amarel computational cluster; and the National Science Foundation MRI Program Award 2117792 for supporting the purchase of a single-crystal X-ray diffractometer employed in this research.

Conflict of Interests

The authors declare no conflict of interest.

Data Availability Statement

The data that support the findings of this study are available in the supplementary material of this article. Deposition Numbers 2295586 (for **1b**), 2295587 (for **2**) contain the supplementary crystallographic data for this paper. These data are provided free of charge by the joint Cambridge Crystallographic Data Centre and Fachinformationszentrum Karlsruhe Access Structures service.

Keywords: anion recognition · host-guest systems · nanocages · perfluorooctanoate · supramolecular chemistry

[1] a) G. Montà-González, F. Sancenón, R. Martínez-Máñez, V. Martí-Centelles, *Chem. Rev.* **2022**, *122*, 13636–13708; b) J. Rebek Jr., *Angew. Chem. Int. Ed.* **2005**, *44*, 2068–2078; c) S. Sarkar, P. Ballester, M. Spektor, E. A. Kataev, *Angew. Chem. Int. Ed.* **2023**, *62*, e202214705; d) M. Han, D. M. Engelhard, G. H. Clever, *Chem. Soc. Rev.* **2014**, *43*, 1848–1860; e) F. J. Rizzuto, L. K. S. von Krbek, J. R. Nitschke, *Nat. Chem. Rev.* **2019**, *3*, 204–222; f) D. Zhang, T. K. Ronson, J. R. Nitschke, *Acc. Chem. Res.* **2018**, *51*, 2423–2436; g) M. Fujita, *Chem. Soc. Rev.* **1998**, *27*, 417–425; h) M. Yoshizawa, J. K. Klosterman, M. Fujita, *Angew. Chem. Int. Ed.* **2009**, *48*, 3418–3438; i) R. Chakrabarty, P. S. Mukherjee, P. J. Stang, *Chem. Rev.* **2011**, *111*, 6810–6918; j) R. A. S. Vasdev, D. Preston, J. D. Crowley, *Chem. Asian J.* **2017**, *12*, 2513–2523; k) L. Zhang, H. Liu, G. Yuan, Y.-F. Han, *Chin. J. Chem.* **2021**, *39*, 2273–2286; l) A. J. McConnell, *Chem. Soc. Rev.* **2022**, *51*, 2957–2971.

[2] a) Y. Yamauchi, M. Yoshizawa, M. Akita, M. Fujita, *Proc. Natl. Acad. Sci. USA* **2009**, *106*, 10435–10437; b) W. Meng, B. Breiner, K. Rissanen, J. D. Thoburn, J. K. Clegg, J. R. Nitschke, *Angew. Chem. Int. Ed.* **2011**, *50*, 3479–3483; c) F. J. Rizzuto, D. M. Wood, T. K. Ronson, J. R. Nitschke, *J. Am. Chem. Soc.* **2017**, *139*, 11008–11011; d) T. K. Ronson, W. Meng, J. R. Nitschke, *J. Am. Chem. Soc.* **2017**, *139*, 9698–9707; e) S. H. A. M. Leenders, R. Becker, T. Kumpulainen, B. de Bruin, T. Sawada, T. Kato, M. Fujita, J. N. H. Reek, *Chem. Eur. J.* **2016**, *22*, 15468–15474; f) E. O. Bobylev, D. A. Poole III, B. de Bruin, J. N. H. Reek, *J. Am. Chem. Soc.* **2022**, *144*, 15633–15642; g) N. Fujita, K. Biradha, M. Fujita, S. Sakamoto, K. Yamaguchi, *Angew. Chem. Int. Ed.* **2001**, *40*, 1718–1721; h) D. A. Rothschild, W. P. Kopcha, A. Tran, J. Zhang, M. C. Lipke, *Chem. Sci.* **2022**, *13*, 5325–5332.

[3] a) J. Lee, S. Lim, D. Kim, O.-S. Jung, Y.-A. Lee, *Dalton Trans.* **2020**, *49*, 15002–15008; b) Y. Wu, C. Zhang, S. Fang, D. Zhu, Y. Chen, C. Ge, H. Tang, H. Li, *Angew. Chem. Int. Ed.* **2022**, *61*, e202209078; c) B. J. J. Timmer, T. J. Mooibroek, *Chem. Commun.* **2021**, *57, 7184–7187*; d) R. L. Paul, S. P. Argent, J. C. Jeffery, L. P. Harding, J. M. Lynam, M. D. Ward, *Dalton Trans.* **2004**, *21*, 3453–3458; e) D. Preston, K. M. Patil, A. T. O. 'Neil, R. A. S. Vasdev, J. A. Kitchen, P. E. Kruger, *Inorg. Chem. Front.* **2020**, *7*, 2990–3001; f) E. Puig, C. Desmarets, G. Gontard, M. N. Rager, A. L. Cooksy, H. Amouri, *Inorg. Chem.* **2019**, *58*, 3189–3195; g) H. T. Chifotides, I. D. Giles, K. R. Dunbar, *J. Am. Chem. Soc.* **2013**, *135*, 3039–3055; h) J. C. Lauer, A. S. Bhat, C. Barwig, N. Fritz, T. Kirschbaum, F. Rominger, M. Mastalerz, *Chem. Eur. J.* **2022**, *28*, e202201527; i) H. Xie, V. W. L. Gunawardana, T. J. Finnegan, W. Xie, J. D. Badjić, *Angew. Chem. Int. Ed.* **2022**, *61*, e202116518; j) A. Ursu, F. P. Schmidtchen, *Angew. Chem. Int. Ed.* **2012**, *51*, 242–246; k) W. J. Ramsay, F. J. Rizzuto, T. K. Ronson, K. Caprice, J. R. Nitschke, *J. Am. Chem. Soc.* **2016**, *138*, 7264–7267; l) S. Löffler, J. Lübben, L. Krause, D. Stalke, B. Dittrich, G. H. Clever, *J. Am. Chem. Soc.* **2015**, *137*, 1060–1063; m) C. García-Simón, M. Garcia-Borràs, L. Gómez, I. Garcia-Bosch, S. Osuna, M. Swart, J. M. Luis, C. Rovira, M. Almeida, I. Imaz, D. Maspoch, M. Costas, X. Ribas, *Chem. Eur. J.* **2013**, *19*, 1445–1456; n) N. Luo, Y.-F. Ao, D.-X. Wang, Q.-Q. Wang, *Angew. Chem. Int. Ed.* **2021**, *60*, 20650–20655; o) S. Freye, J. Hey, A. Torras-Galán, D. Stalke, R. Herbst-Irmer, M. John, G. H. Clever, *Angew. Chem. Int. Ed.* **2012**, *51*, 2191–2194; p) D. Van Craen, M. G. Kalarikkal, J. J. Holstein, *J. Am. Chem. Soc.* **2022**, *144*, 18135–18143.

[4] a) C. Sgarlata, J. S. Mugridge, M. D. Pluth, B. E. F. Tiedemann, V. Zito, G. Arena, K. N. Raymond, *J. Am. Chem. Soc.* **2010**, *132*, 1005–1009; b) W. Zhang, D. Yang, J. Zhao, L. Hou, J. L. Sessler, X.-J. Yang, B. Wu, *J. Am. Chem. Soc.* **2018**, *140*, 5248–5256; c) D. L. Caulder, R. E. Powers, T. N. Parac, K. N. Raymond, *Angew. Chem. Int. Ed.* **2004**, *37*, 1840–1843; d) F. Jia, H. Hupatz, L.-P. Yang, H. V. Schröder, D.-H. Li, S. Xin, D. Lentz, F. Witte, X. Xie, B. Paulus, C. A. Schalley, W. Jiang, *J. Am. Chem. Soc.* **2019**, *141*, 4468–4473; e) T. N. Parac, D. L. Caulder, K. N. Raymond, *J. Am. Chem. Soc.* **1998**, *120*, 8003–8004; f) S. M. Butterfield, J. Rebek, *J. Am. Chem. Soc.* **2006**, *128*, 15366–15367; g) J. S. Mugridge, R. G. Bergman, K. N. Raymond, *J. Am. Chem. Soc.* **2012**, *134*, 2057–2066; h) M. D. Pluth, D. W. Johnson, G. Szigethy, A. V. Davis, S. J. Teat, A. G. Oliver, R. G. Bergman, K. N. Raymond, *Inorg. Chem.* **2009**, *48*, 111–120.

[5] a) W. Xuan, M. Zhang, Y. Liu, Z. Chen, Y. Cui, *J. Am. Chem. Soc.* **2012**, *134*, 6904–6907; b) S. Tashiro, M. Kobayashi, M. Fujita, *J. Am. Chem. Soc.* **2006**, *128*, 9280–9281; c) Y. Li, J. Dong, W. Gong, X. Tang, Y. Liu, Y. Cui, Y. Liu, *J. Am. Chem. Soc.* **2021**, *143*, 20939–20951; d) Y. Hatakeyama, T. Sawada, M. Kawano, M. Fujita, *Angew. Chem. Int. Ed.* **2009**, *48*, 8695–8698; e) D. Fujita, K. Suzuki, S. Sato, M. Yagi-Utsumi, Y. Yamaguchi, N. Mizuno, T. Kumasaka, M. Takata, M. Noda, S. Uchiyama, K. Kato, M. Fujita, *Nat. Commun.* **2012**, *3*, 1093.

[6] a) F. J. Rizzuto, J. P. Carpenter, J. R. Nitschke, *J. Am. Chem. Soc.* **2019**, *141*, 9087–9095; b) A. Schmidt, V. Molano, M. Hollering, A. Pöthig, A. Casini, F. E. Kühn, *Chem. Eur. J.* **2016**, *22*, 2253–2256; c) W. Cullen, S. Turega, C. A. Hunter, M. D. Ward, *Chem. Sci.* **2015**, *6*, 625–631.

[7] a) C. G. P. Taylor, J. R. Piper, M. D. Ward, *Chem. Commun.* **2016**, *52*, 6225–6228; b) C. R. P. Fulong, M. G. E. Guardian, D. S. Aga, T. R. Cook, *Inorg. Chem.* **2020**, *59*, 6697–6708; c) I. A. Riddell, M. M. J. Smulders, J. K.

Clegg, J. R. Nitschke, *Chem. Commun.* **2011**, *47*, 457–459; d) C. G. P. Taylor, A. J. Metherell, S. P. Argent, F. M. Ashour, N. H. Williams, M. D. Ward, *Chem. Eur. J.* **2020**, *26*, 3065–3073; e) L. Ma, C. J. E. Haynes, A. B. Grommet, A. Walczak, C. C. Parkins, C. M. Doherty, L. Longley, A. Tron, A. R. Stefankiewicz, T. D. Bennett, J. R. Nischke, *Nat. Chem.* **2020**, *12*, 270–275; f) Y. Ruan, H. A. Taha, R. J. Yoder, V. Maslak, C. M. Hadad, J. D. Badjić, *J. Phys. Chem. B.* **2013**, *117*, 3240–3249.

[8] a) J. L. Bolliger, A. M. Belenguer, J. R. Nitschke, *Angew. Chem. Int. Ed.* **2013**, *52*, 7958–7962; b) E. G. Percástegui, *Chem. Commun.* **2022**, *58*, 5055–5071; c) H. Omorodion, M. Palenzuela, M. Ruether, B. Twamley, J. A. Platts, R. J. Baker, *New J. Chem.* **2018**, *42*, 7956–7968; d) Z. Zheng, H. Yu, W.-C. Geng, X.-Y. Hu, Y.-Y. Wang, Z. Li, Y. Wang, D.-S. Guo, *Nat. Commun.* **2019**, *10*, 5762; e) Y. He, D. Luo, V. M. Lynch, M. Ahmed, J. L. Sessler, X. Chi, *Chem* **2023**, *9, 93–101*; f) Z. Chen, Y.-L. Lu, L. Wang, J. Xu, J. Zhang, X. Xu, P. Cheng, S. Yang, W. Shi, *J. Am. Chem. Soc.* **2023**, *145*, 260–267.

[9] a) L.-J. Wang, S. Bai, Y.-F. Han, *J. Am. Chem. Soc.* **2022**, *144*, 16191–16198; b) Y.-J. Hou, K. Wu, Z.-W. Wei, K. Li, Y.-L. Lu, C.-Y. Zhu, J.-S. Wang, M. Pan, J.-J. Jiang, G.-Q. Li, C.-Y. Su, *J. Am. Chem. Soc.* **2018**, *140*, 18183–18191; c) L. Mei, P. Ren, Q.-y. Wu, Y.-b. Ke, J.-s. Geng, K. Liu, X.-q. Xing, Z.-w. Huang, K.-q. Hu, Y.-l. Liu, L.-y. Yuan, G. Mo, Z.-h. Wu, J. K. Gibson, Z.-f. Chai, W.-q. Shi, *J. Am. Chem. Soc.* **2020**, *142*, 16538–16545; d) B.-N. T. Nguyen, J. D. Thoburn, A. B. Grommet, D. J. Howe, T. K. Ronson, H. P. Ryan, J. L. Bolliger, J. R. Nitschke, *J. Am. Chem. Soc.* **2021**, *143*, 12175–12180.

[10] a) A. S. Braegelman, M. J. Webber, *Theranostics* **2019**, *9*, 3017–3040; b) J. E. M. Lewis, E. L. Gavey, S. A. Cameron, J. D. Crowley, *Chem. Sci.* **2012**, *3*, 778–784; c) F. Schmitt, J. Freudenreich, N. P. E. Barry, L. Juillerat-Jeanneret, G. Süss-Fink, B. Therrien, *J. Am. Chem. Soc.* **2012**, *134*, 754–757; d) Y.-R. Zheng, K. Suntharalingam, T. C. Johnstone, S. J. Lippard, *Chem. Sci.* **2015**, *6*, 1189–1193; e) B. Woods, R. D. M. Silva, C. Schmidt, D. Wragg, M. Cavaco, V. Neves, V. F. C. Ferreira, L. Gano, T. S. Morais, F. Mendes, J. D. G. Correia, A. Casini, *Bioconjugate Chem.* **2021**, *32*, 1399–1408.

[11] a) C. J. Brown, F. D. Toste, R. G. Bergman, K. N. Raymond, *Chem. Rev.* **2015**, *115*, 3012–3035; b) D. Samanta, S. Mukherjee, Y. P. Patil, P. S. Mukherjee, *Chem. Eur. J.* **2012**, *18*, 12322–12329; c) M. Yoshizawa, M. Tamura, M. Fujita, *Science* **2006**, *312*, 251–254; d) D. H. Leung, D. Fiedler, R. G. Bergman, K. N. Raymond, *Angew. Chem. Int. Ed.* **2004**, *43*, 963–966; e) K. Kanagaraj, R. Wang, M.-K. Zhao, P. Ballester, J. Rebek Jr., Y. Yu, *J. Am. Chem. Soc.* **2023**, *145*, 5816–5823; f) A. Dhamija, A. Gunnam, X. Yu, H. Lee, I.-C. Hwang, Y. Ho Ko, K. Kim, *Angew. Chem. Int. Ed.* **2022**, *61*, e202209326; g) M. Morimoto, S. M. Bierschenk, K. T. Xia, R. G. Bergman, K. N. Raymond, F. D. Toste, *Nat. Catal.* **2020**, *3*, 969–984; h) T. A. Bender, R. G. Bergman, K. N. Raymond, F. D. Toste, *J. Am. Chem. Soc.* **2019**, *141*, 11806–11810; i) C. M. Hong, R. G. Bergman, K. N. Raymond, F. D. Toste, *Acc. Chem. Res.* **2018**, *51*, 2447–2455.

[12] a) M. Yamashina, M. M. Sartin, Y. Sei, M. Akita, S. Takeuchi, T. Tahara, M. Yoshizawa, *J. Am. Chem. Soc.* **2015**, *137*, 9266–9269; b) O. Yanshyna, M. J. Białek, O. V. Chashchikhin, R. Klajn, *Commun. Chem.* **2022**, *5*, 44; c) H. Liu, C. Guo, Z. Zhang, C. Mu, Q. Feng, M. Zhang, *Chem. Eur. J.* **2023**, *29*, e202203926; d) Y. Hou, Z. Zhang, S. Lu, J. Yuan, Q. Zhu, W.-P. Chen, S. Ling, X. Li, Y.-Z. Zheng, K. Zhu, M. Zhang, *J. Am. Chem. Soc.* **2020**, *142*, 18763–18768; e) G. Wu, Y. Chen, S. Fang, L. Tong, L. Shen, C. Ge, Y. Pan, X. Shi, H. Li, *Angew. Chem. Int. Ed.* **2021**, *60*, 16594–16599; f) A. J. Plajer, E. G. Percástegui, M. Santella, F. J. Rizzuto, Q. Gan, B. W. Laursen, J. R. Nitschke, *Angew. Chem. Int. Ed.* **2019**, *58*, 4200–4204.

[13] a) W. Liu, S. Bobbala, C. L. Stern, J. E. Hornick, Y. Liu, A. E. Enciso, E. A. Scott, J. F. Stoddart, *J. Am. Chem. Soc.* **2020**, *142*, 3165–3173; b) L. Cao, M. Šekutor, P. Y. Zavalij, K. Mlinarić-Majerski, R. Glaser, L. Isaacs, *Angew. Chem. Int. Ed.* **2014**, *53*, 988–993.

[14] a) G. Szalóki, V. Croué, V. Carré, F. Aubriet, O. Alévêque, E. Levillain, M. Allain, J. Aragó, E. Ortí, S. Goeb, M. Sallé, *Angew. Chem. Int. Ed.* **2017**, *56*, 16272–16276; b) D. Zhang, T. K. Ronson, S. Güryel, J. D. Thoburn, D. J. Wales, J. R. Nitschke, *J. Am. Chem. Soc.* **2019**, *141*, 14534–14538; c) M. Han, R. Michel, B. He, Y.-S. Chen, D. Stalke, M. John, G. H. Clever, *Angew. Chem. Int. Ed.* **2013**, *52*, 1319–1323; d) T. Y. Kim, R. A. S. Vasdev, D. Preston, J. D. Crowley, *Chem. Eur. J.* **2018**, *24*, 14878–14890; e) R. Djemili, L. Kocher, S. Durot, A. Peuronen, K. Rissanen, V. Heitz, *Chem. Eur. J.* **2019**, *25*, 1481–1487; f) W. Cullen, K. A. Thomas, C. A. Hunter, M. D. Ward, *Chem. Sci.* **2015**, *6*, 4025–4028.

[15] a) M. Zenka, J. Preinl, E. Pertermann, A. Lützen, K. Tiefenbacher, *Eur. J. Inorg. Chem.* **2023**, *26*, e202300110; b) D. Zhang, T. K. Ronson, J. Mosquera, A. Martinez, L. Guy, J. R. Nitschke, *J. Am. Chem. Soc.* **2017**, *139*, 6574–6577; c) T. Y. Kim, L. Digal, M. C. Gardiner, N. T. Lucas, J. D. Crowley, *Chem. Eur. J.* **2017**, *23*, 15089–15097; d) M. D. Wise, J. J. Holstein, P. Pattison, C. Besnard, E. Solari, R. Scopelliti, G. Bricogne, K. Severin, *Chem. Sci.* **2015**, *6*, 1004–1010.

[16] a) F. Biedermann, H.-J. Schneider, *Chem. Rev.* **2016**, *116*, 5216–5300; b) S. L. Cockroft, C. A. Hunter, *Chem. Soc. Rev.* **2007**, *36*, 172–188; c) F. J. Carver, C. A. Hunter, F. J. Carver, E. M. Seward, *Chem. Commun.* **1998**, 775–776; d) G. Tobajas-Curiel, Q. Sun, J. K. M. Sanders, P. Ballester, C. A. Hunter, *Chem. Sci.* **2023**, *14*, 6226–6236.

[17] a) S. Pullen, J. Tessarolo, G. H. Clever, *Chem. Sci.* **2021**, *12*, 7269–7293; b) J. E. M. Lewis, *Chem. Commun.* **2022**, *58*, 13873–13886.

[18] a) C. Z. Woods, H.-T. Wu, C. Ngai, B. de Camara, R. R. Julian, R. J. Hooley, *Dalton Trans.* **2022**, *51*, 10920–10929.1451 C; b) P. M. Bogie, T. F. Miller, R. J. Hooley, *Isr. J. Chem.* **2018**, *58*, 130–139.

[19] a) M. M. Smulders, I. A. Riddell, C. Browne, J. R. Nitschke, *Chem. Soc. Rev.* **2013**, *42*, 1728–1754; b) M. Dekhtiarenko, G. Szalóki, V. Croué, J. Bou Zeid, D. Canevet, M. Allain, V. Carré, F. Aubriet, Z. Voitenko, M. Sallé, S. Goeb, *Org. Chem. Front.* **2023**, *10*, 1803–1810; c) S.-C. Li, L.-X. Cai, M. Hong, Q. Chen, Q.-F. Sun, *Angew. Chem. Int. Ed.* **2022**, *61*, e202204732; d) Y. Fang, T. Murase, S. Sato, M. Fujita, *J. Am. Chem. Soc.* **2013**, *135*, 613–615; e) A. K. Bar, S. Mohapatra, E. Zangrando, P. S. Mukherjee, *Chem. Eur. J.* **2012**, *18*, 9571–9579.

[20] a) K. G. Dutton, D. A. Rothschild, D. B. Pastore, T. J. Emge, M. C. Lipke, *Inorg. Chem.* **2020**, *59*, 12616–12624; b) I. F. Mansoor, K. G. Dutton, D. A. Rothschild, R. C. Remsing, M. C. Lipke, *J. Am. Chem. Soc.* **2021**, *143*, 16993–17003; c) P. T. Blackburn, I. F. Mansoor, K. G. Dutton, A. M. Tyryshkin, M. C. Lipke, *Chem. Commun.* **2021**, *57*, 11342–11345; d) P. T. Blackburn, M. C. Lipke, *J. Coord. Chem.* **2022**, *75*, 1520–1542.

[21] C. A. Hunter, H. L. Anderson, *Angew. Chem. Int. Ed.* **2009**, *48*, 7488–7499.

[22] P. Thordarson, *Chem. Soc. Rev.* **2011**, *40*, 1305–1323.

[23] M. M. J. Smulders, S. Zarra, J. R. Nitschke, *J. Am. Chem. Soc.* **2013**, *135*, 7039–7046.

[24] a) E. M. Sunderland, X. C. Hu, C. Dassuncao, A. K. Tokranov, C. C. Wagner, J. G. Allen, *J. Expo. Sci. Environ. Epidemiol.* **2019**, *29*, 131–147; b) D. Q. Andrews, O. V. Naidenko, *Environ. Sci. Technol. Lett.* **2020**, *7*, 931–936.

[25] a) S. Komine, S. Takahashi, T. Kojima, H. Sato, S. Hiraoka, *J. Am. Chem. Soc.* **2019**, *141*, 3178–3186; b) F. Ibukuro, T. Kusukawa, M. Fujita, *J. Am. Chem. Soc.* **1998**, *120*, 8561–8562; c) X. Zhang, S. Takahashi, K Aratsu, I. Kikuchi, H. Sato, S. Hiraoka, *Phys. Chem. Chem. Phys.* **2022**, *24*, 2997–3006; d) T. Tateishi, S. Takahashi, I. Kikuchi, K. Aratsu, H. Sato, S. Hiraoka, *Inorg. Chem.* **2021**, *60*, 16678–16685.

[26] The crystal structure of **2** bears an improper S_2 rotation axis, rather than a proper C_2 rotation axis. However, the S_2 axis still results in pseudo-2-fold symmetric environment in the solid state that matches the ^{1}H NMR characterization of **2**.

[27] a) A. Stone, E. B. Fleischer, *J. Am. Chem. Soc.* **1968**, *90*, 2735–2748; b) C. J. Kingsbury, M. O. Senge, *Coord. Chem. Rev.* **2021**, *431*, 213760.

[28] a) Bindfit can be found at: http://supramolecular.org/; b) D. B. Hibbert, P. Thordarson, *Chem. Commun.* **2016**, *52*, 12792–12805.

[29] We attempted to quantify the strong association of the *p*-tolyl guests into **1a**,**b** in MeCN via UV-vis, fluorescence, and isothermal titration calorimetry, but none of these methods proved fruitful for revealing guest affinities in our systems. Instead, competition studies were monitored by NMR where the difference in affinity between guests (or hosts) is within the range measurable by NMR ($K_{rel} < 10^5$).

[30] B. G. Cox, in *Acids and Bases: Solvent Effects on Acid-Base Strength, 1st ed.;* OUP Oxford, United Kingdom **2013**, Ch. 9.

[31] A. Kütt, S. Tshepelevitsh, J. Saame, M. Lõkov, I. Kaljurand, S. Selberg, I. Leito, *Eur. J. Org. Chem.* **2021**, *2021*, 1407–1419.

[32] A. L. B. Formiga, A. F. Nogueira, K. Araki, H. E. Toma, *New J. Chem.* **2008**, *32*, 1167–1174.

[33] B. D. McCarthy, D. J. Martin, E. S. Rountree, A. C. Ullman, J. L. Dempsey, *Inorg. Chem.* **2014**, *53*, 8350–8361.

[34] R. Guo, X. Qi, H. Xiang, P. Geaneotes, R. Wang, P. Liu, Y.-M. Wang, *Angew. Chem. Int. Ed.* **2020**, *59*, 16651–16660.

[35] H. Nagae, R. Aoki, S.-n. Akutagawa, J. Kleemann, R. Tagawa, T. Schindler, G. Choi, T. P. Spaniol, H. Tsurugi, J. Okuda, K. Mashima, *Angew. Chem. Int. Ed.* **2018**, *57*, 2492–2496.

[36] M. Hulla, D. Ortiz, S. Katsyuba, D. Vasilyev, P. J. Dyson, *Chem. Eur. J.* **2019**, *25*, 11074–11079.

[37] Y. Pei, J. Ma, F. Song, Y. Zhao, Z. Li, H. Wang, J. Wang, R. Du, *J. Mol. Liq.* **2022**, *366*, 120256.

[38] H. Yi, P. Hu, S. A. Snyder, *Angew. Chem. Int. Ed.* **2020**, *59*, 2674–2678.

[39] E. C. Sutton, C. E. McDevitt, J. Y. Prochnau, M. V. Yglesias, A. M. Mroz, M. C. Yang, R. M. Cunningham, C. H. Hendon, V. J. DeRose, *J. Am. Chem. Soc.* **2019**, *141*, 18411–18415.

[40] W. R. Dolbier, *Guide to Fluorine NMR for Organic Chemists.* Wiley: Hoboken, NJ, **2008**.
[41] L. Allouche, A. Marquis, J.-M. Lehn, *Chem. Eur. J.* **2006**, *12*, 7520–7525.
[42] G. M. Sheldrick, SADABS - *Bruker Nonius Area Detector Scaling and Absorption Correction*, Bruker-AXS Inc.: Madison, Wisconsin, **2003**.
[43] G. M. Sheldrick, *Acta Crystallogr. Sect. A* **2008**, *64*, 112–122.
[44] G. M. Sheldrick, *SHELXL97, Program for Crystal Structure Refinement*, University of Göttingen: Germany, **1997**.
[45] N. Barooah, B. C. Pemberton, A. C. Johnson, J. Sivaguru, *Photochem. Photobiol. Sci.* **2008**, *7*, 1473–1479.

Manuscript received: September 15, 2023
Accepted manuscript online: October 31, 2023
Version of record online: November 14, 2023